

AD-A079 545

BRISTOL UNIV (ENGLAND) H H WILLS PHYSICS LAB
THE PHYSICAL MECHANISMS RESPONSIBLE FOR THE WEATHERING OF EPOXY--ETC(U)
OCT 79 C ALEXANDRE, T W TURNER, K H ASHBEE

F/6 11/9

DA-ERO-78-6-117

NL

UNCLASSIFIED

1 OF 1
AD
A079545



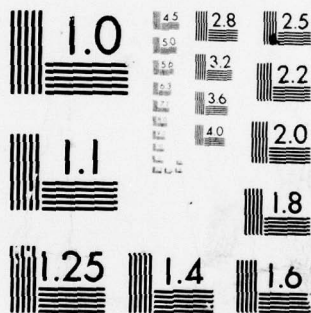
END

DATE

FILMED

3-80

DDC



MICROCOPY RESOLUTION TEST CHART
NATIONAL BUREAU OF STANDARDS-1963-A

DA 079545

DDC FILE COPY

(12)

LEVEL A

The Physical Mechanisms Responsible for
the Weathering of Epoxy Resins and GFR Epoxy Resins

Annual Technical Report

by

C. Alexandre
T. W. Turner
K. H. G. Ashbee

October 1979

EUROPEAN RESEARCH OFFICE
United States Army
London England

GRANT NUMBER DA-ERO-78-G-117

H. H. Wills Physics Laboratory
University of Bristol

DDC
RECEIVED
JAN 17 1980
A

Approved for Public Release: distribution unlimited

80 1 17 004

UNCLASSIFIED

SECURITY CLASSIFICATION OF THIS PAGE (When Data Entered)

R&D 2605

REPORT DOCUMENTATION PAGE		READ INSTRUCTIONS BEFORE COMPLETING FORM
1. REPORT NUMBER	2. GOVT ACCESSION NO.	3. RECIPIENT'S CATALOG NUMBER
4. TITLE (and Subtitle) The Physical Mechanisms Responsible for the Weathering of Epoxy Resins and GFR Epoxy Resins.		5. TYPE OF REPORT & PERIOD COVERED Annual Technical Report. Oct 78 - Oct 79
7. AUTHOR(s) C. Alexandre, T.W. Turner, K.H.G. Ashbee		8. CONTRACT OR GRANT NUMBER(s) DAERO-78-G-117
9. PERFORMING ORGANIZATION NAME AND ADDRESS US Army R&S Gp (Eur) Box 65, FPO NY 09510		10. PROGRAM ELEMENT, PROJECT, TASK AREA & WORK UNIT NUMBERS 11T161102BH57
11. CONTROLLING OFFICE NAME AND ADDRESS University of Bristol H.H. Wills Physics Laboratory, Bristol, U.K.		12. REPORT DATE Oct 1979
14. MONITORING AGENCY NAME & ADDRESS (if different from Controlling Office) 12 34		15. SECURITY CLASS. (of this report) Unclassified
16. DISTRIBUTION STATEMENT (of this Report) Distribution Unlimited; approved for Public Release		
17. DISTRIBUTION STATEMENT (of the abstract entered in Block 20, if different from Report)		
18. SUPPLEMENTARY NOTES		
19. KEY WORDS (Continue on reverse side if necessary and identify by block number) (U) Weathering (U) Ultrasonic Photoelasticity (U) Epoxy Resins (U) NDT of Composites		
20. ABSTRACT (Continue on reverse side if necessary and identify by block number) Experiments are described where the cylindrically symmetric fields associated with the fibre/resin interface are explored by examination in the optical microscope. The patterns of birefringence show how the difference of the principal stresses vary with distance from the fibre. Changes in the load transfer at the interface during hot water uptake have been detected. Specimens examined include E and S glass fibres totally embedded in epoxy resin slabs as well as 1 mm thick transverse sections through a unidirectional		

DD FORM 1 JAN 73 1473

EDITION OF 1 NOV 65 IS OBSOLETE

UNCLASSIFIED

393 113

SECURITY CLASSIFICATION OF THIS PAGE (When Data Entered)

20, Contd,

composite.

The ultrasonic photoelastic method has given way to a more direct approach to investigate SiO_2 /epoxy resin interfaces, where epoxy coated X-cut slabs of quartz are stimulated piezoelectrically and the resonant mechanical vibration examined. Attempts to incorporate the quartz slabs into the transducer in visualization experiments have so far failed to produce fringes.

Investigation of the swelling inhomogeneity that accompanies the pattern of water uptake is described; a model specimen consisting of a microscope cover slip bonded to a rigid block of glass is brought into contact with an optical flat. The displacement of the cover slip, on swelling of the resin by water absorption, can be observed by the interference patterns. Moire fringes, produced by superimposing photographs taken before and after the changes, faithfully reveal the resin swelling geometry.

The computer model to simulate the stress fields is described. A finite element approach is taken treating the fibre as purely elastic in an elastoplastic resin matrix. The aim is to treat the interfacial region as a third phase of finite dimensions.

TABLE OF CONTENTS

Section		Page
	SUMMARY	
	LIST OF FIGURES	
	LIST OF TABLES	
1.	INTRODUCTION	1.
2.	DEBONDING OF FIBRES IN AN EPOXY RESIN MATRIX	3.
3.	ULTRASONIC PHOTOELASTICITY	6.
	3.1. COMPUTER MODEL	6.
	3.2. QUARTZ OSCILLATOR	6.
4.	STRESS FIELDS	8.
	4.1. INTERFERENCE EXPERIMENTS	8.
	4.2. FINITE ELEMENTS	9.
5.	CONCLUSIONS	12.
	REFERENCES	

Accession For	
NTIS Grant	<input checked="" type="checkbox"/>
DDC TAB	<input type="checkbox"/>
Unannounced	<input type="checkbox"/>
Justification	<input type="checkbox"/>
E:	
Distribution/	
Availability Codes	
Dist	Avail and/or special
A	

LIST OF FIGURES

No.

1. Stress birefringence pattern for an 'E' glass fibre (10 μ dia.) embedded in MY 750 resin.
2. Stress birefringence in a 1mm thick transverse section through a unidirectional composite.
3. Load transfer index versus immersion time in water at 80°C for an 'E' glass fibre in MY 750 resin.
4. Retardation versus immersion time in water at 100°C for an 'E' glass fibre in MY 750 resin.
5. Shape changes in the fillet of resin between three closely packed fibres.
6. Moiré patterns for MY 750 resin immersed in water at 60°C showing the ingress of swelling during water uptake.
7. Migration distance of the 1st Moiré fringe, shown in figure 6, plotted against the square root of time.
8. 22-element mesh
9. 236-element mesh
10. 1% biaxial tensile strain, small fibre, low plasticity interface.
11. 1% biaxial tensile strain, small fibre, high plasticity interface.
12. 1% biaxial tensile strain, large fibre, low plasticity interface.
13. 1% biaxial tensile strain, large fibre, medium plasticity interface.
14. 1% pure shear strain, small fibre, low plasticity interface.
15. 1% pure shear strain, small fibre, high plasticity interface.

LIST OF TABLES

No.

1. Loss of load transfer by various composite specimens during exposure to water.

1. INTRODUCTION

The experimental work done during this reporting period has been close to the origins of "composites variability" and the data presented in this report reflect the consequences of such. Changes in resin/fibre load transfer during hot water uptake have been detected by direct observation of changes in optical retardation measured through adjacent diameters of individual short fibres. The fibres used fall into two categories. Firstly, fibres which have permitted comparisons between the performances of fibres drawn in chemically unreactive atmospheres and the performances of commercial fibres of the same E and S glass compositions. These comparisons reveal some differences in behaviour between clinically drawn and commercially drawn fibres, although it has not yet been established whether or not surface layer impurities and/or the surface treatments applied to the commercial fibres accelerate the mechanism(s) responsible for loss of load transfer attributable to diffused water in the absence of externally applied stress. Nor has it been established whether commercial fibre surface treatments mitigate interfacial attack by water. The epoxy resins used for the above experiments were CIBA-GEIGY MY 750 and MY 720.

The second category of materials used in the present experimental investigations were samples of short S2 glass fibres in SP 250 epoxy resin. These samples were taken from the flash of a composite panel manufactured at AMMRC and, unlike apparently identical samples prepared for optical microscopy studies, they are transparent. Optical retardation measurements have revealed no significant difference in behaviour during water immersion between these samples and the S2/MY 750 samples described above.

Ultrasonic photoelasticity investigations have proceeded through the year in an attempt to get more precise data from property changes attributable to water uptake. By the very nature of its modes of propagation, ultrasound samples a very much larger region of material than that which can be sensibly identified as "the interface" and, for this reason, the technique is more sensitive to macroscopic changes such as matrix plasticisation than it is to localised changes such as the destruction of bonds at fibre/matrix interfaces.

The analytical approach of stress fields arising from differential contraction between fibre and resin materials and of modifications to those stress fields that result from resin swelling during water uptake has been superseded by the finite element method. The

finite element method (f.e.m.) due to Adams (1970) treats the purely elastic fibre and elastoplastic matrix in generalized plane strain and provides for a pseudo-three-dimensional stress analysis. The method adopted here is that developed by Alexander and Turner (1975) for axisymmetric flow and has been modified in order to accommodate plane strain. The interface is represented by a third phase. The analysis so far attempted diverges very little from that already reported by Adams.

Realistic numbers for parameters to be fed into the f.e.m. computer model are being generated by experimental measurement. Thus, gradation of resin swelling in model uniaxial composites that have been exposed to aqueous environments is determined by measuring optical birefringence in successive transverse sections.

2. DEBONDING OF FIBRES IN AN EPOXY RESIN MATRIX

When an epoxy resin system cures, it shrinks and generates stresses in and around inclusions such as totally embedded short fibres. The stress fields are cylindrically symmetric with compressive stresses acting normally across the fibre/resin interface and compressive stresses acting both longitudinally and radially within the fibre. These components of stress can be explored by examination in the optical microscope using polarised light. Figure 1 shows the pattern of birefringence in and around an 'E' glass fibre, totally embedded in a slab of CIBA-GEIGY MY 750 epoxy resin. The fibre axis is aligned parallel to one of the crossed polars. The stress within the fibre includes a component which arises from shear stress transferred at the interface and which builds up with distance from each fibre end. For long fibres a condition of plane strain is reached in the central regions as shown by the constancy of stress birefringence in the central region for the fibre shown in figure 1.

The resin adjacent to a fibre experiences a hoop tensile stress as well as the radial compressive stress referred to above. The magnitudes of both components fall off with distance from the fibre as demonstrated by figure 2 which shows the pattern of stress birefringence in a 1 mm thick transverse section through a unidirectional composite. The fibres are arranged in a rectangular array to facilitate direct comparison of the stress fields with those computed by the finite element model. The specimens used for this study require careful preparation. In particular, the spacing between fibres must be large enough to permit resolution of several stress isochromatics.

The effects on interfacial load transfer of exposure of composites to aqueous environments can be detected by monitoring differences between optical retardations measured through neighbouring diameters in individual fibres. Ashbee and Wyatt (1969) have defined as a practical load transfer index, the difference between the retardation measured through a diameter at the centre of a fibre and that measured through a diameter near the fibre end. Any deterioration in the ability to transfer shear stress across the interface reduces the build up of axial fibre stress and this is reflected by a decrease in magnitude of the index. Measurements of load transfer index versus time of immersion in water at 80°C are shown in figure 3, for an MY 750 epoxy resin matrix. The mean of two retardations measured in the epoxy resin adjacent to the ends of a fibre in a composite immersed in water at 100°C is shown as a function of time in figure 4. Both sets of data reflect the variability of composite materials.

Data for a selection of experiments performed to seek evidence of differences in loss of load transfer by various composite specimens during exposure to water are summarised in table 1.

RESIN	FIBRE	WATER TEMPERATURE	TIME TAKEN TO DEBOND
MY 750	Carbon 'A'	22°C	no debonding in 81 days
	Carbon 'A'	100°C	~ 9 hours
	Carbon 'H'	22°C	no debonding in 81 days
	Carbon 'H'	100°C	~ 15 minutes
	'E' glass (NH ₃ drawn)	22°C	40-53 days
	'E' glass (NH ₃ drawn) coupled*	22°C	40-53 days
	'E' glass (NH ₃ drawn)	100°C	< 1½ hours
	'E' glass (NH ₃ drawn) coupled*	100°C	~ 1¼ hours
	'S' glass (NH ₃ drawn)	22°C	36-49 days
	'S' glass (NH ₃ drawn) coupled*	22°C	36-49 days
	'S' glass (NH ₃ drawn)	100°C	22 hours
	'S' glass (NH ₃ drawn) coupled*	100°C	22 hours
SP 250	S2 glass	22°C	25 days
	S2 glass	80°C	1-5 days
MY 720	'S' glass (NH ₃ drawn)	22°C	9 days
	'E' glass (NH ₃ drawn)	22°C	9 days
	456 (S2) glass	22°C	8 days
	P263A (S2) glass	22°C	8 days
	801 (L) glass	22°C	not debonded in 8 days
	H + S 904 (S1) glass	22°C	not debonded in 8 days
	S glass (NH ₃ drawn)	80°C	< 20½ hours
	456 (S2) glass	80°C	1-2 hours
	P263A (S2) glass	80°C	1 hour
	801 (L) glass	80°C	1-2 hours
	H+S 904 (S1) glass	80°C	1-4 days

*Fibres coated with silane coupling agent, A187, manufactured by Union Carbide.

Table 1. Loss of load transfer by various composite specimens during exposure to water.

3. ULTRASONIC PHOTOELASTICITY

The photoelastic method for imaging ultrasound (reported in the Final Technical Report by T. W. Turner and K. H. G. Ashbee, grant No. DA-ERO-76-G-068) has been used to look for material property changes at and near glass/epoxy interfaces. Experimental difficulties encountered include (a) rapid attenuation of the ultrasound signal and (b) poor resolution arising from the frequency which, at ~ 2 MHz, is somewhat low for "collecting" data. It was subsequently decided that the interface might be more easily studied in specimens of single crystal quartz and epoxy resin. Changes in mechanical damping characteristics during water uptake should be revealed by using such resin coated quartz piezoelectric crystals to drive the transducer in visualization experiments. To date, no fringes have been recorded.

3.1 COMPUTER MODEL

The computer model, described in Final Technical Report of DA-ERO-76-G-068, has been developed to include the interface and now has improved graphics. The principal thrust has been directed towards NDT and will be reported elsewhere, Kitson, Low and Turner (1979).

3.2 QUARTZ OSCILLATOR

The state of localised stress near the interfacial region that is introduced during curing precludes the direct observation of ultrasonic fringes in the resin. Successful application of the technique is restricted to observation of fringes, in an adjacent stress free visualizing block, i.e. remote from the specimen. In order to investigate SiO_2 /epoxy resin interfaces more directly, a series of experiments have been carried out where the PZT 5A piezoelectric discs are replaced by crystalline quartz. X-cut slabs, 2 mm thick, were sawn from a synthetic quartz single crystal having a cross-sectional area of about 2 cm^2 . The slabs were then polished, cleaned and coated with 1 mm of CIBA-GEIGY MY 750 epoxy resin. An electric field up to 800 v. was applied across the epoxy/quartz/epoxy with aluminium foil electrodes, and then shorted using a thyristor. The resonant mechanical vibration, observed on an

oscilloscope, begins with an amplitude of ~ 15 v. and decays in about 15 cycles. The measured frequency is typically 39 MHz which is more than an order of magnitude higher than the expected frequency of 1.44 MHz. This unexpected result has not been explained, since the thyristor voltage cut off rate was designed to give the major Fourier component at about 1.5 MHz. The interfacial debonding on boiling the specimens in distilled water modifies the frequency trace by changing the relative pulse heights. This takes the form of modulation of the 39 MHz frequency by a second frequency close to 39 MHz. The energy emanating from the quartz slabs so far investigated is not sufficient to drive a transducer for ultrasound visualization.

4. STRESS FIELDS

4.1 INTERFERENCE EXPERIMENT

At the 1978 ARO/AMMRC review of composites research, Professor D. Adams presented a finite element model for the stress field in a uni-directional composite that has experienced uniform differential thermal contraction between fibre and matrix materials and uniform swelling of matrix material following water uptake. The flux of diffused water received by the fillet of resin located between a bundle

of closely packed fibres, figure 5, is not isotropic. Of special interest, because of its proximity to the resin/fibre interface, is the Ω - shaped film of resin between two adjacent fibres. In the absence of wicking, the curved surfaces of this film are shielded from water by the presence of the fibres, i.e. water uptake is restricted to diffusion parallel to these curved surfaces. To investigate the swelling inhomogeneity that accompanies this pattern of water uptake and hence calculate the inhomogeneous elastic field created if (as is nearly true in a real composite) the resin is constrained not to swell, a model specimen consisting of a microscopic cover slip bonded with epoxy resin to a massive and therefore rigid block of glass, has been prepared. When the free surface of the cover slip is brought into contact with an optical flat, a pattern of Newton's rings is formed in the gap trapped between them. Should the shape of the gap change, as happens when the resin absorbs water, swells and displaces the cover slip, the pattern of Newton's rings changes and superposition of photographs taken before and after the changes produces a set of Moiré fringes which faithfully reveals the geometry of the resin swelling.

Figure 6 shows a sequence of photographs for a square specimen manufactured using MY 750 epoxy resin. The cover slip was approximately $150\ \mu\text{m}$ thick and the resin layer approximately $50\ \mu\text{m}$ thick. All glass surfaces were thoroughly cleaned before specimen assembly. Water uptake was achieved by immersing the specimen in distilled water at 60°C . From the distribution of fringes it is evident that the swelling is strongly inhomogeneous and that it faithfully reflects the geometry of the specimen for a considerable length of time. It should be noted that a Moiré fringe having moved and been replaced by its neighbour represents an increase in thickness due to swelling of $\lambda/2$, i.e. a percentage increase of approximately 0.5%. (The broad fringes running across the centre of the specimen and seen towards the later stages of the test are a result of the specimen tilting relative to the optical flat. With improved temperature control it is anticipated that such fringes will be substantially eliminated). In figure 7 the position of the first Moiré fringe is plotted as a function of $(\text{time})^2$. Since this fringe corresponds to a relatively large water concentration its migration is relatively slow and only the early stages of its progression are recorded. For points near to the rim and

midway along a specimen side, a linear relationship is expected if resin swelling is governed by Fickian behaviour. Within the limits of experimental error, the relationship is linear.

4.2 FINITE ELEMENTS

The classical f.e.m. paper of Turner, Clough, Martin and Topp (1956) has been developed and extended principally by Zienkiewicz (1977) and, for application the microscopic behaviour of fibre composites, by the University of Wyoming group. The principles of the displacement formulation of the f.e.m. for plane strain have been applied to the program using triangular elements and linear shape functions. Figure 8 shows the mesh used for developing the program. The region bounded by nodes 1, 5, 7, 9, 1 represent the fibre with the remaining mesh representing the epoxy resin matrix. Figure 9 shows a more realistic mesh with fibre bounded by 1, 19, 35, 1, where the region 19, 36, 52, 35, 19 may be treated as interfacial, again with the remainder representing the matrix. The mesh of Figure 9 with 236 elements and 137 nodes is generated logically in the computer. This enables the mesh to be modified for larger fibres, for interface manipulation, and for shape changes. This last point is regarded as particularly important since in the form shown, i.e. a square, the symmetry may be too high for real composites: changing the right angle of the mesh to an arbitrary value or 60° say, is easily achieved. Both mesh dimensions are 7 microns square, corresponding to a fibre diameter of 9.3 microns and a fibre volume ratio of 39%.

The strain in an element as a function of the nodal displacements is given by the strain shape matrix $[B]_e$, the suffix e relating to a single element. The use of a linear displacement shape function leads to a $[B]_e$ independent of x and y, and a constant elemental strain. Linearity of the displacement function and the coupling of neighbouring elements at nodal points ensures continuity of displacement across element boundaries, and compatibility conditions are automatically fulfilled.

There is a matrix $[D]_e$ which, when multiplied by the strain vector, gives the stress vector derived in terms of the elastic constants. The stress system is equivalent to a set of forces acting at the nodes of the element. The force vector $\{F\}_e$ may be expressed as

$$\{F\}_e = [B]_e^T [D]_e [B]_e \{a\}_e$$

where $\{a\}_e$ is the displacement vector.

$$\text{or } \{F\}_e = [K]_e \{a\}_e$$

where $[K]_e$ is a 6 x 6 matrix called the elemental stiffness matrix.

Corresponding to this equation is a global stiffness equation

$$\{F\} = [K] \{a\}$$

where the two vectors represent the forces and displacements at every node in the mesh. The displacement vector is found by inversion of the stiffness matrix when the loading condition is formulated in terms of known forces, and unknown forces can be calculated from known displacements. Strains and stresses may then be calculated.

The fibre is treated as purely elastic whereas the resin matrix is considered to be stressed beyond yield and into the plastic region, i. e. resin plastic strain must be added to resin elastic strain. Thus, in the program, loads are applied in increments which follow the plastic stress-strain curve by evaluating a new stiffness matrix for each new increment. Displacements and strains are calculated for each increment as in the elastic situation. The method is known as the tangent modulus method because the stress-strain matrix is found by using, instead of Young's Modulus, the tangent to the $\sigma - \epsilon$ curve at a given strain. The von Mises yield criterion is assumed together with the Prandtl-Reuss flow rule. Initially the whole load is applied to solve for the elastic formulation and if any elements are stressed beyond the yield criterion, all quantities are reduced in proportion to bring them within the elastic regime. The program then proceeds by loading incrementally where, at the end of each increment, the incremental strains are added to the current components of strain and new equivalent stresses and strains are calculated.

The stage has been reached where the program is functioning well for elastoplastic matrix resin and elastic fibre, and the first results for biaxial tensile strain and pure shear are shown in the Figures 10-15. Figure 10 shows the final mesh shape superimposed on the initial undeformed mesh for a 1% biaxial tensile strain. The resin matrix has the properties of an epoxy resin containing a water concentration of 2% and is referred to in the legend as 'low plasticity'. The crossed lines inside each element indicate the orientation and relative magnitudes of the principal stresses, the program having been written so that the vector lengths fit inside the smallest element. Figure 11 distinguishes a third phase, in that the row of elements adjacent to the fibres have properties of an epoxy resin containing a water concentration of 6%, the

remaining matrix still containing 2% water, and is referred to as a 'high plasticity interface'. Figure 12 is similar to Figure 10 except that the fibre has been enlarged by including an extra row of elements in the fibre, and demonstrates the mesh flexibility. Figure 13 is similar to Figure 11 but with the enlarged fibre and with the row of elements adjacent to the fibre containing 4% moisture. Figures 14 and 15 show the consequences of a 1% extension in the x-direction combined with a 1% compression in the y-direction, i.e. the consequences of macroscopic pure shear. Compressive principal stress vectors are barred at their ends.

5. CONCLUSIONS

1. By comparing optical retardation measurements made through parallel diameters in individual fibres in order to detect interfacial load transfer, it has been demonstrated that the behaviour of epoxy resin composites during hot water uptake is different for different fibre chemistries. Not only are there differences between 'E' glass and 'S' glass fibre composites, but also between commercial and "contaminant free" fibres of each glass composition.
2. S2/SP250 composites, prepared with the resin components mixed in accordance with the manufacturer's recommendations for a stoichiometric mix, are not sufficiently transparent for optical retardation experiments of the kind reported in conclusion 1.
3. An S2/SP250 composite panel fabricated at AMMRC is bounded by a flash which contains a low volume fraction of short fibres and which, since it is transparent, is eminently suitable for optical retardation experiments to measure times for loss of load transfer during water uptake. At 80°C, fibres lying parallel to and ~100 μ m from the external surface lose their load transfer ability after ~80 hours.
4. Using photoelastic visualization of ultrasound, it is possible to provide a visual display of the effects of water uptake on ultrasound velocities in composite materials.
5. The swelling associated with water uptake by resin samples having geometries representative of regions of resin in real composites, is strongly inhomogeneous. The magnitudes of the corresponding swelling stresses (10's of bars) are of the same order as those due to differential contraction between resin and glass during cooling from the cure temperature.
6. It is possible to take into account flow (due to plasticisation by water, for example) when computer modelling the self-stress fields in composites.
7. Using measured differences in the magnitudes of radial and tangential principal stresses, it appears that computer modelling of the true (inhomogeneous) self-stress fields of wet composites is feasible.

REFERENCES

- Adams, D. F., (1970). "Inelastic analysis of a unidirectional composite subjected to transverse normal loading." *J. Composite Materials*, 4, 310.
- Alexander, J. M. and Turner, T. W., (1975). "An investigation of the die-less drawing of titanium and some steels." 15th International M. T. D. R. Conference, Birmingham, England.
- Ashbee, K. H. G., and Wyatt, R. C., (1969) "Water damage in glass fibre/resin composites." *Proc. R. Soc. A.*, 312, 553.
- Kitson, N. K., Low, S. A., and Turner, T. W. (1979). "Photoelastic visualization experiments and a computer model for non-destructive testing." Ultrasonics International 79 Conference, Graz, Austria.
- Turner, M. J., Clough, R. W., Martin, H. C., and Topp, L. J., (1956), "Stiffness and deflection analysis of complex structures," *J. Aero. Sci.*, 23, 805.
- Zienkiewicz, O. C., (1977), "The finite element method," McGraw Hill.

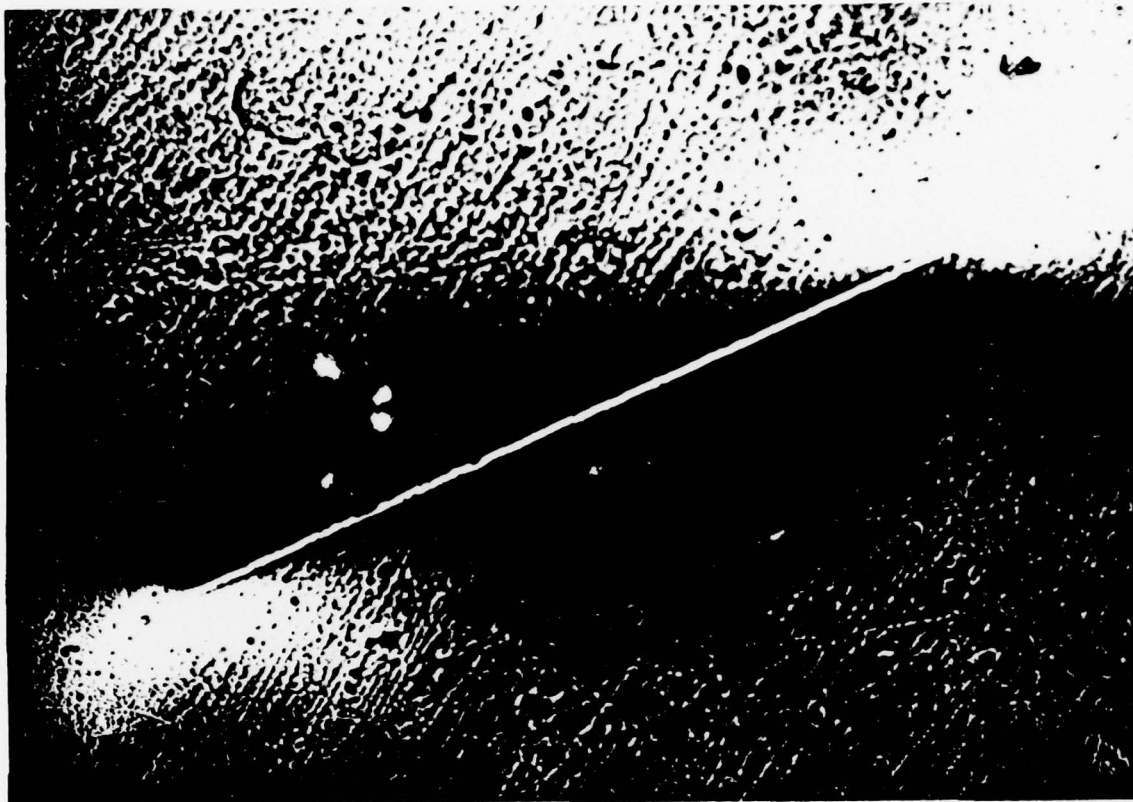


Figure 1. Stress birefringence pattern for an 'E' glass fibre ($10\text{ }\mu\text{ dia.}$) embedded in MY 750 resin.



Figure 2. Stress birefringence in a 1mm thick transverse section through a unidirectional composite.

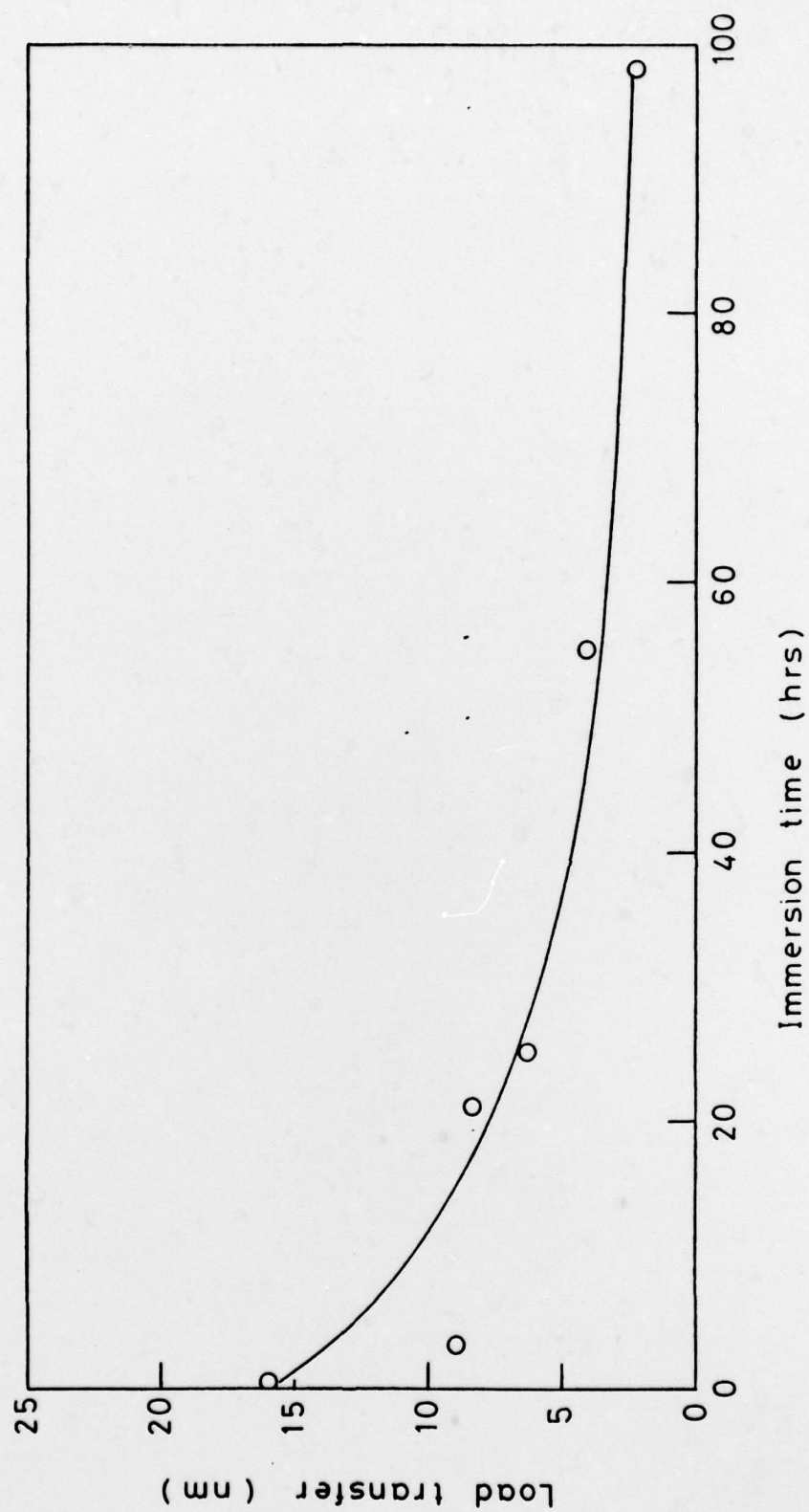


Figure 3. Load transfer index versus immersion time in water at 80°C for an 'E' glass fibre in MY 750 resin.

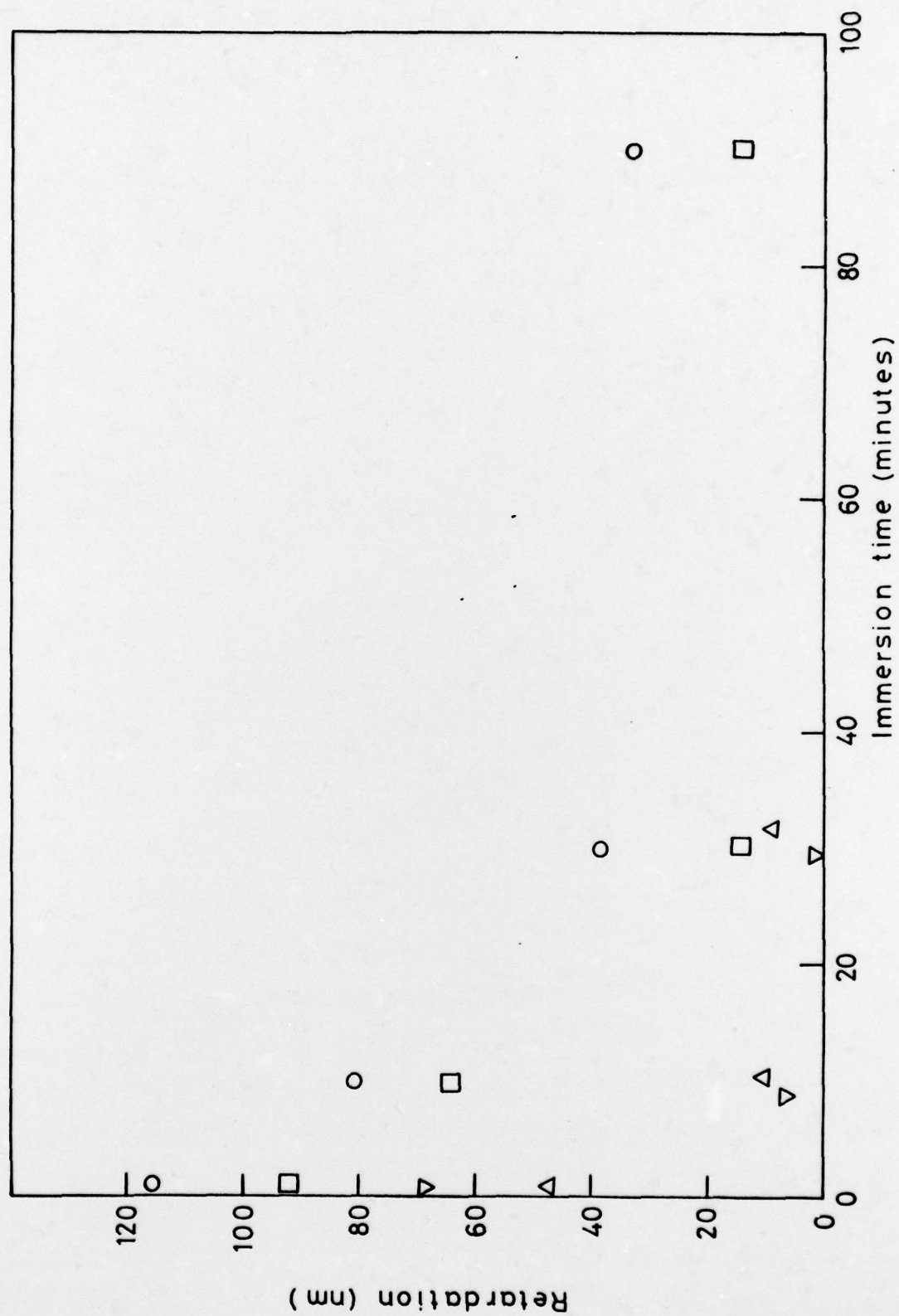
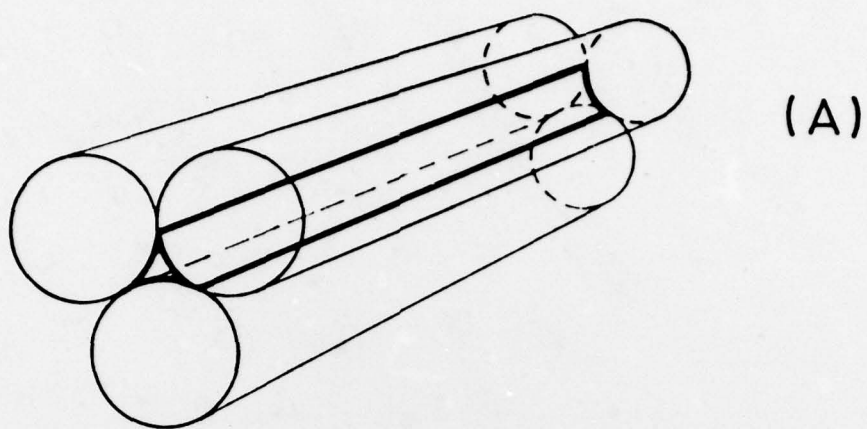
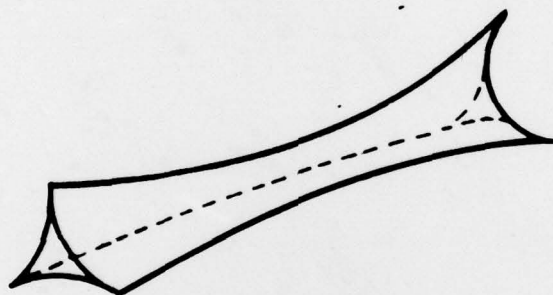


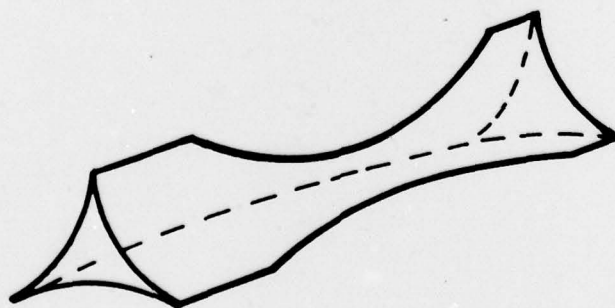
Figure 4. Retardation versus immersion time in water at 100°C for an 'E' glass fibre in MY 750 resin.



(A)

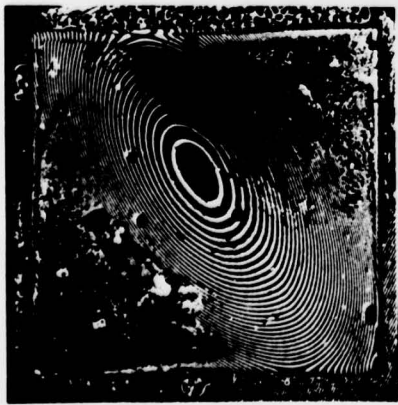


(B)



(C)

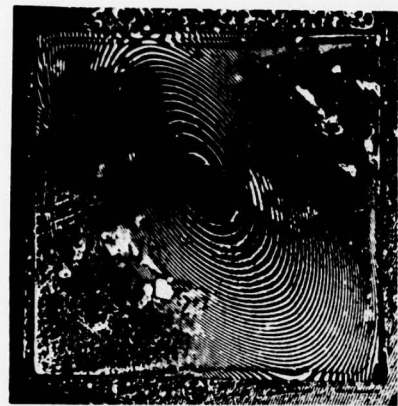
Figure 5. Shape changes in the fillet of resin between three closely packed fibres.



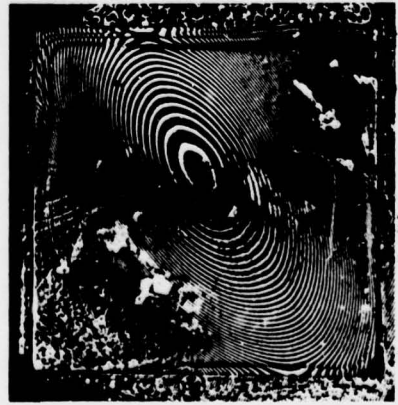
6.5 Hrs



23 Hrs



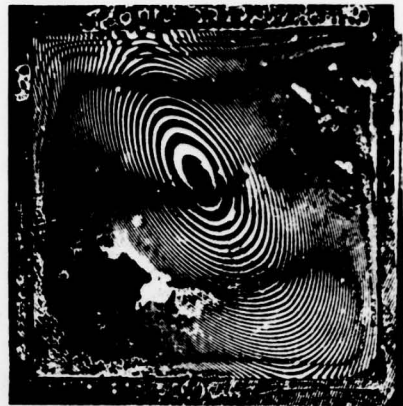
31 Hrs



47 Hrs



72 Hrs



144 Hrs

Figure 6. Moiré patterns for MY 750 resin immersed in water at 60°C showing the ingress of swelling during water uptake.

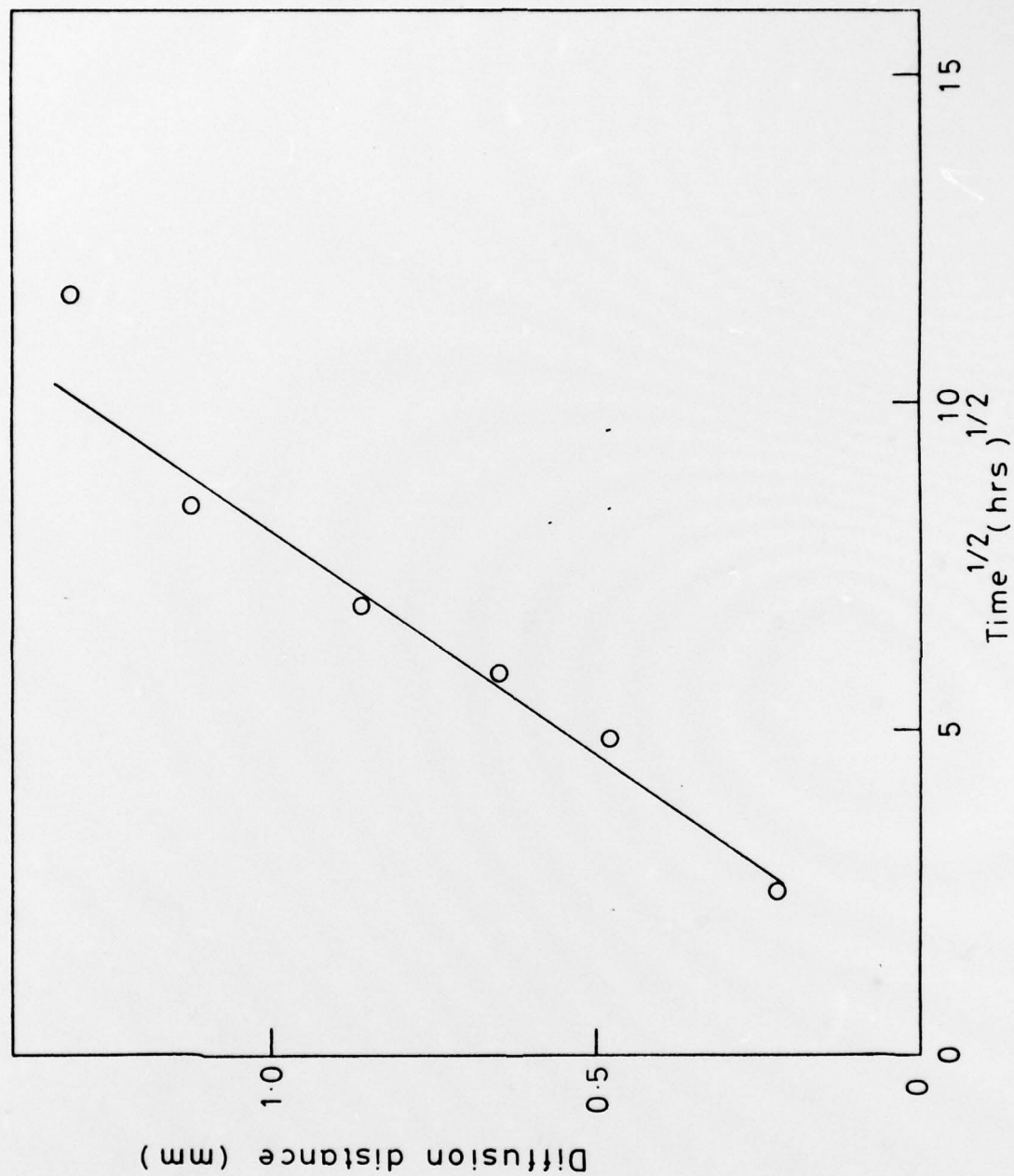
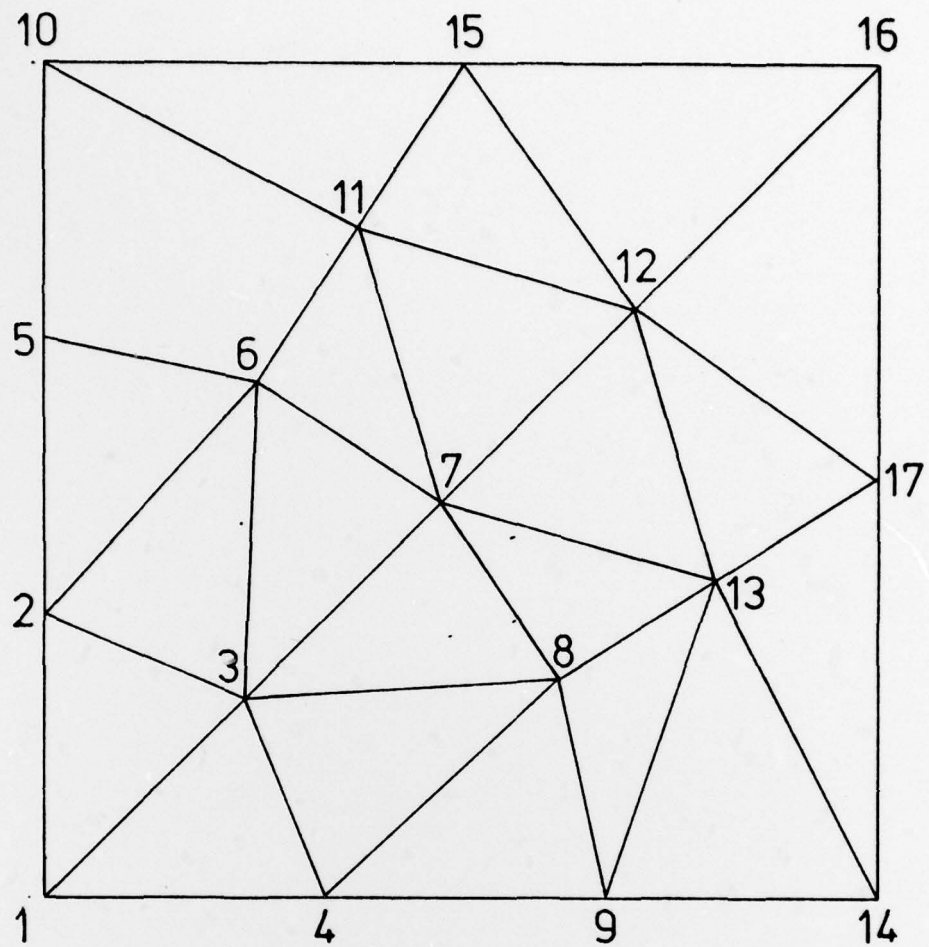


Figure 7. Migration distance of the 1st Moiré fringe, shown in figure 6, plotted against the square root of time.



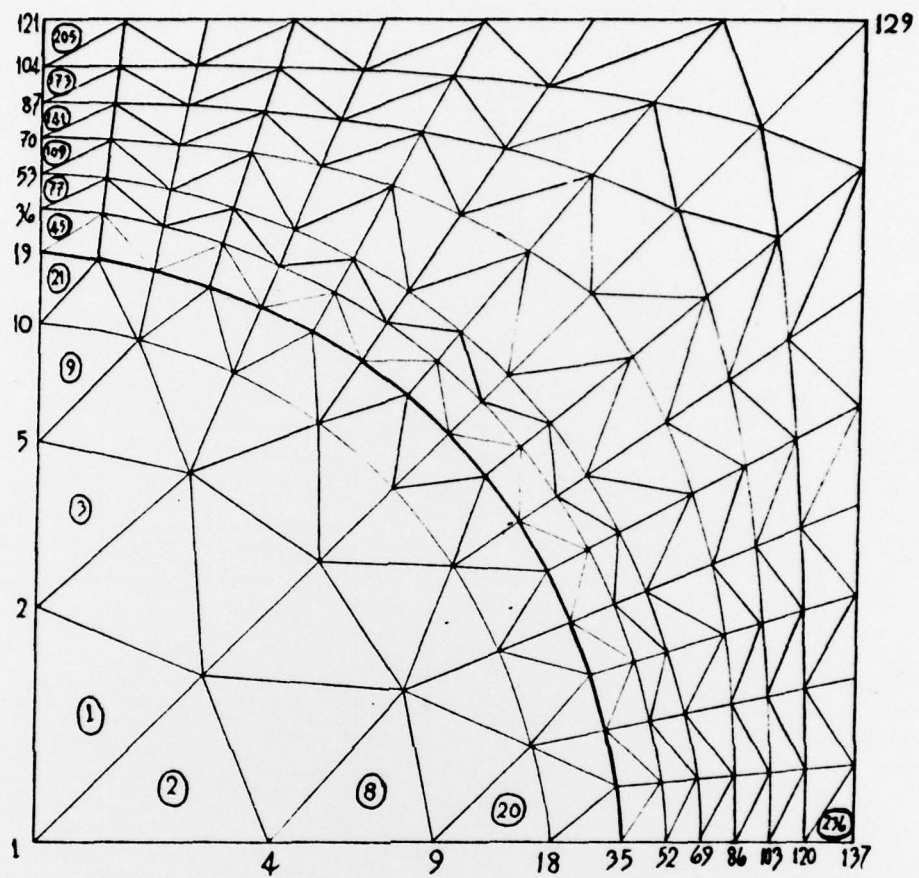


Figure 9. 236-element mesh

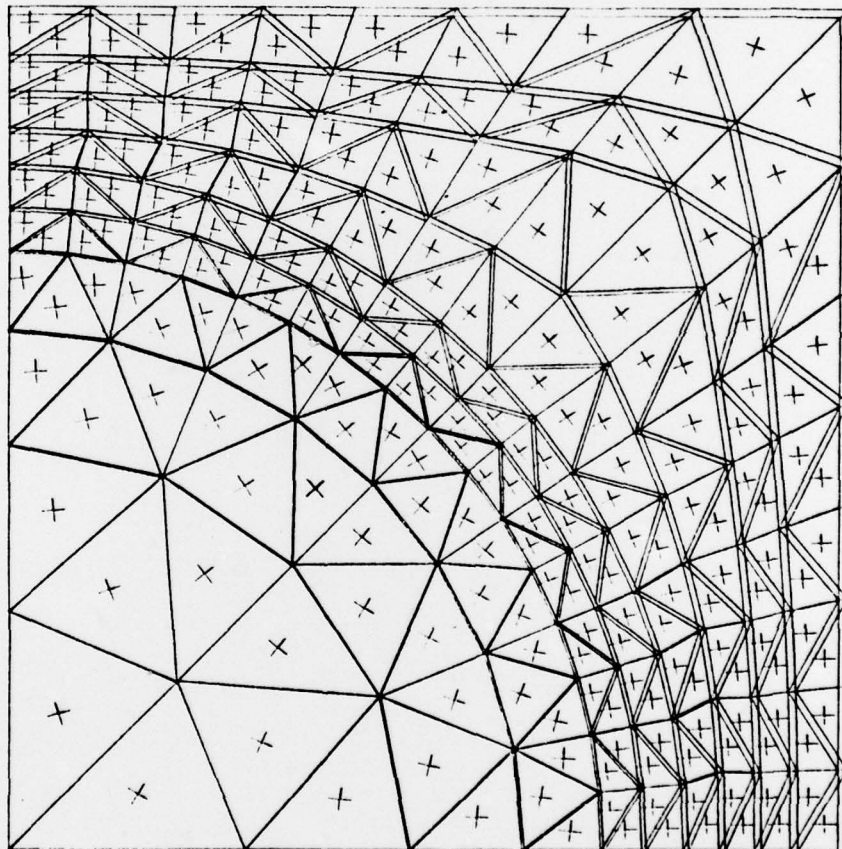


Fig. 10. 1% Biaxial tensile strain, small fibre, low plasticity interface.

Stresses in element 1 are: 96.7 M Pa and 96.9 M Pa.

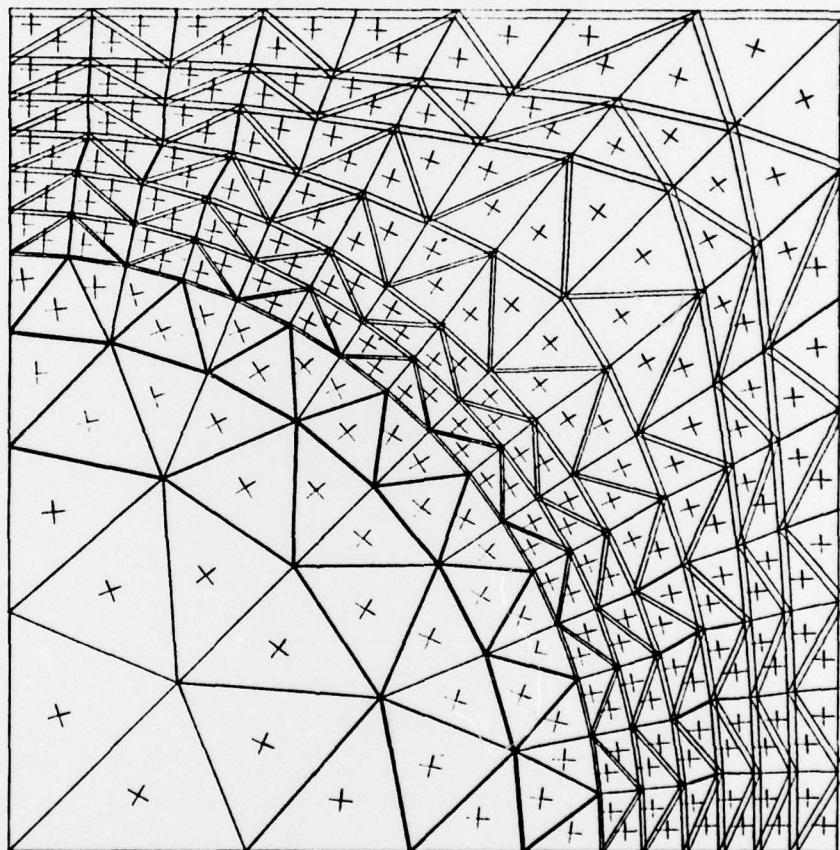


Fig. 11. 1% Biaxial tensile strain, small fibre,
high plasticity interface.

Stresses in element 1 are: 93.1 M Pa and 93.3 M Pa.

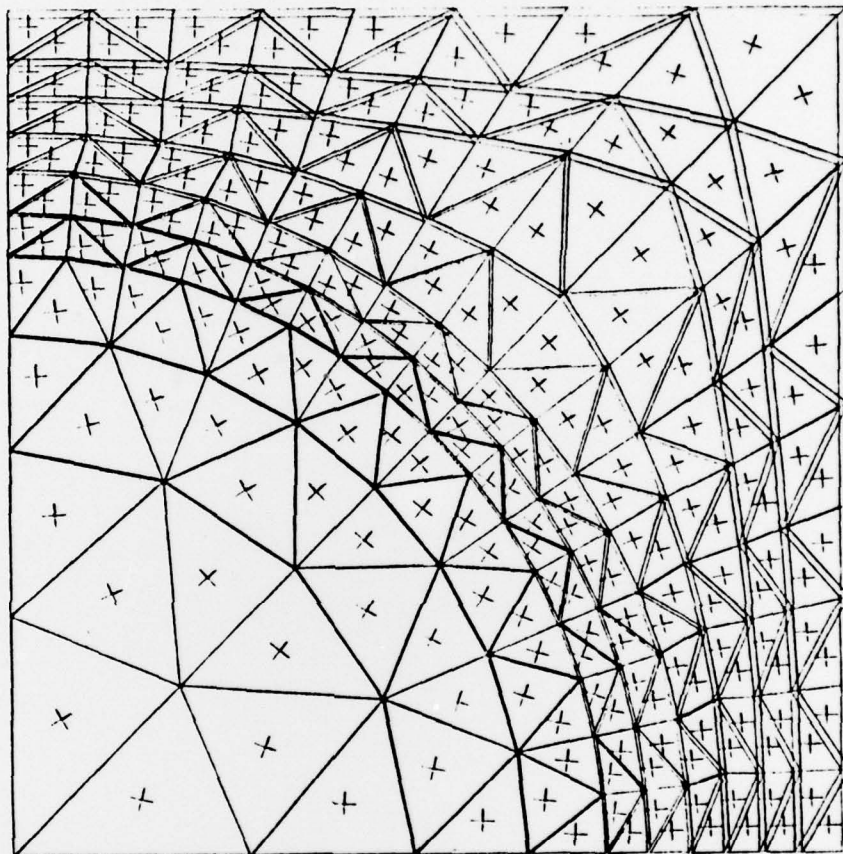


Fig. 12. 1% Biaxial tensile strain, large fibre,
low plasticity interface.

Stresses in element 1 are: 145 M Pa and 145 M Pa .

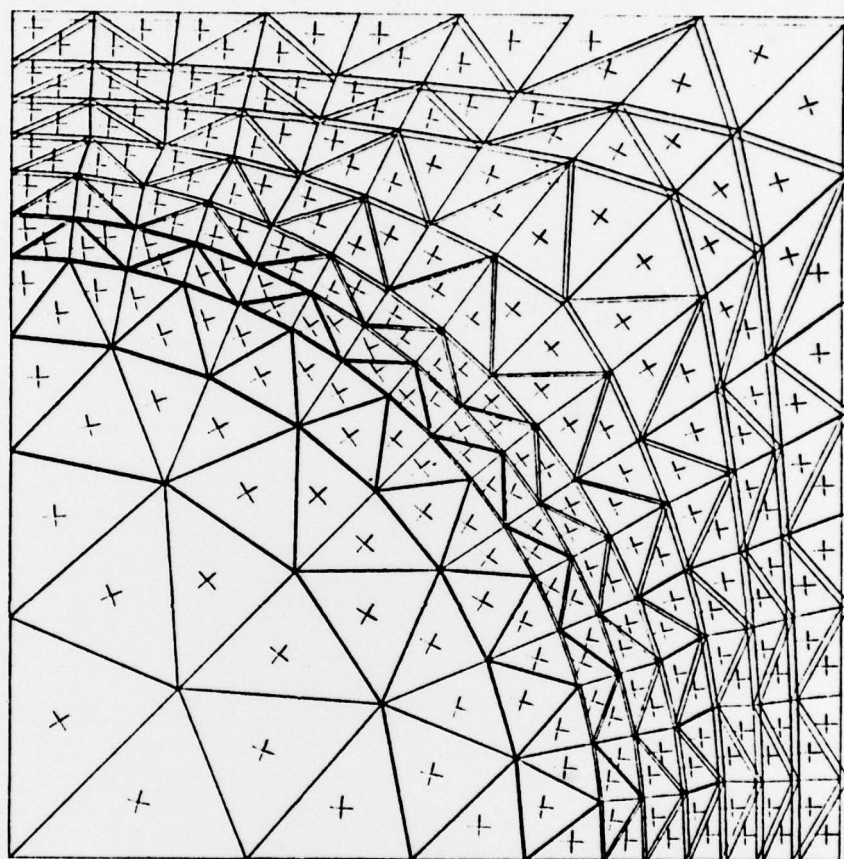


Fig. 13. 1% Biaxial tensile strain, large fibre,
medium plasticity interface.

Stresses in element 1 are: 143 M Pa and 143 M Pa.

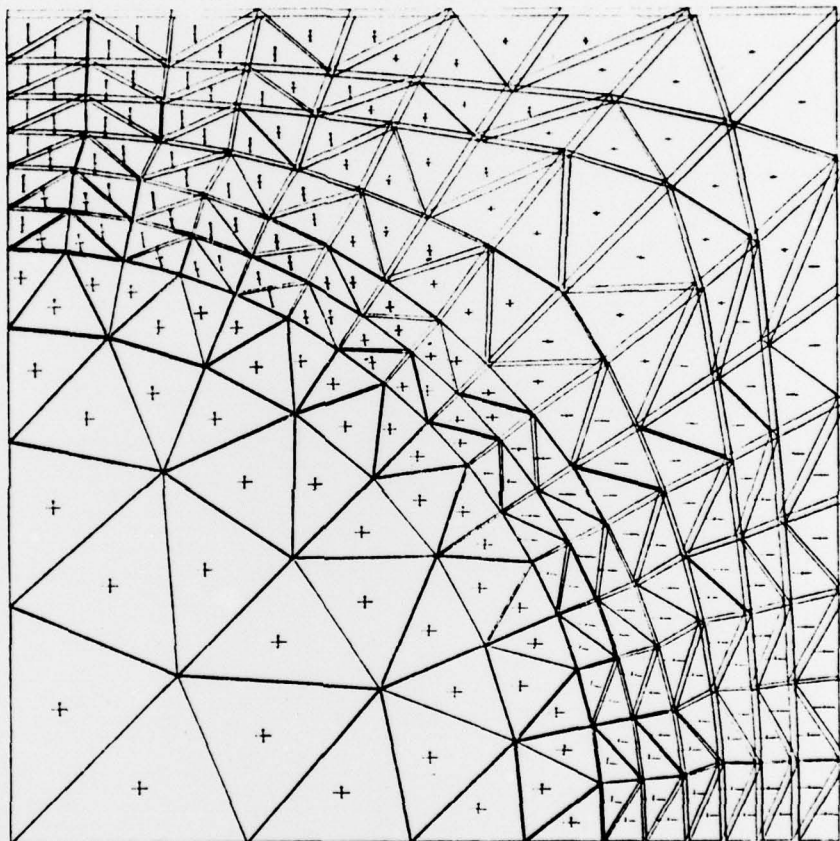


Fig. 14. 1% Pure shear strain, small fibre,
low plasticity interface.

Stresses in element 1 are: 47.7 M Pa and -37.4 M Pa.
Vectors with bars denote compressive stresses.

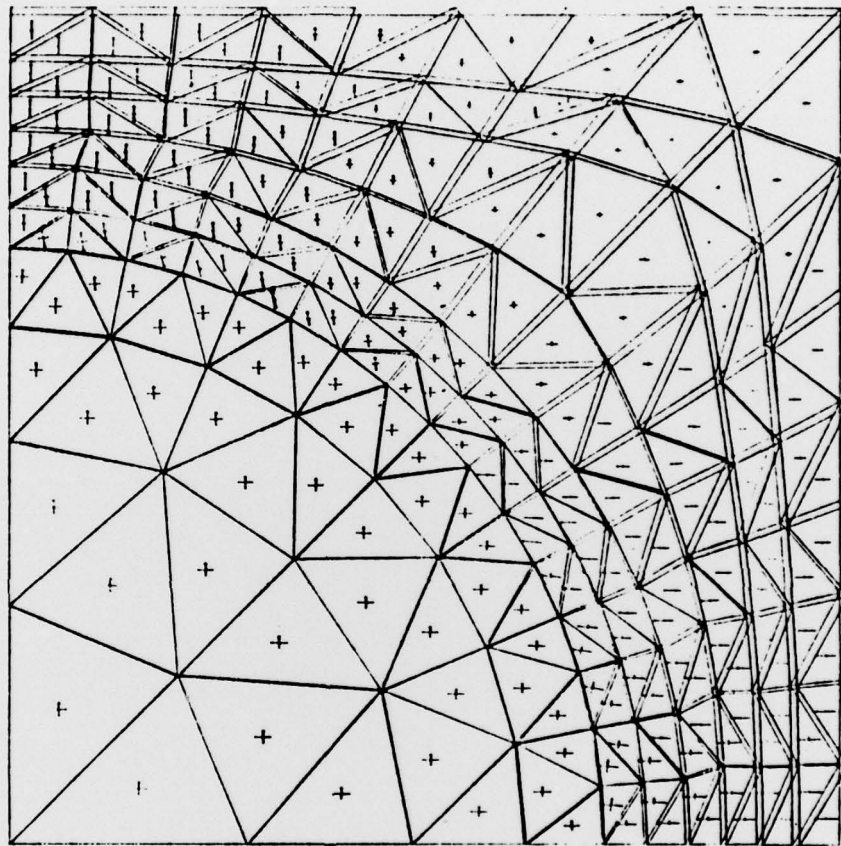


Fig. 15. 1% Pure shear strain, small fibre,
high plasticity interface.

Stresses in element 1 are 45.6 M Pa and -36.0 M Pa.
Vectors with bars denote compressive stresses.